

Supporting Information

High-performance SERS chips for sensitive identification and detection of antibiotic residues based on self-assembled hollow Ag octahedrons

Lu Tan ^{a,b}, Yongbing Lou ^{a,*}, Jun-Jie Zhu ^{b,c,*}

^a School of Chemistry and Chemical Engineering, Southeast University, Nanjing, Jiangsu 211189, China

^b State Key Laboratory of Analytical Chemistry for Life Science, School of Chemistry and Chemical Engineering, Nanjing University, Nanjing, Jiangsu 210023, China

^c Shenzhen Research Institute of Nanjing University, Shenzhen 518000, China

**Corresponding author. E-mail: lou@seu.edu.cn (Y. Lou), jjzhu@nju.edu.cn (J.-J. Zhu)*

Experimental section	4
Chemical and materials.	4
Characterization of materials.	4
Synthesis of the Cu ₂ O templates.	5
Fabrication of the hollow Ag superstructures.	5
Preparation of close-packed hollow Ag superstructures.	5
SERS measurement of the probes on substrates.	6
Synthesis of the Ag nanoparticles.	6
The calculations of enhancement factor (EF).	6
The calculation of limit of detection (LOD) and relative standard deviation (RSD)....	7
Adsorption capacity.	7
SERS detection of CIP, AMX and CZL in different water samples.....	8
SERS detection of ENR in milk.....	8
Fig. S1	9
Fig. S2	9
Fig. S3	9
Fig. S4	10
Fig. S5	10
Fig. S6	11
Fig. S7	11
Fig. S8	12
Fig. S9	13
Fig. S10	13
Fig. S11	14
Fig. S12	15
Fig. S13	15
Fig. S14	16
Table S1	17
Table S2	18

Table S3	19
Table S4	20
Table S5	21
Table S6	22
References	23

Experimental section

Chemical and materials.

All of the chemical reagents used in this experiment were of analytical grade and used without further purification. Copper chloride dihydrate ($\text{CuCl}_2 \cdot 2\text{H}_2\text{O}$), ethanol, polyvinylpyrrolidone-K30 (PVP-K30), sodium hydroborate (NaBH_4), acetic acid (CH_3COOH) and hexane were acquired from Sinopharm Chemical Reagent Co., Ltd. L-ascorbic acid (AA), trisodium citrate dihydrate (TSC), sodium hydroxide (NaOH), crystal violet (CV), copper (II) phthalocyanine (CuPc) and silver nitrate (AgNO_3) were purchased from Aladdin-Reagent Co., Ltd. Methylene blue (MB), amoxicillin (AMX), norfloxacin (NOR), enrofloxacin (ENR), ciprofloxacin (CIP), cefazolin (CZL), malachite green (MG) and doxycycline hydrochloride (DCH) were purchased from Shanghai Macklin Biochemical Co., Ltd. The Sylgard184 PDMS elastomer base and curing agent was obtained from Dow Corning Corporation (Michigan, USA). The milk sample was purchased from a local supermarket. Ultrapure water (18 M Ω cm, Millipore) was used to prepare all of aqueous solutions throughout the work.

Characterization of materials.

The crystal structure and phase of the samples were characterized by X-ray diffraction (XRD) patterns, which were performed from 10 ° to 80 ° (5 ° min⁻¹) on Bruker Advanced D8 X-ray diffractometer using Cu K α radiation source. The morphologies, microstructures and energy-dispersive analysis of X-ray (EDX) were recorded on Hitachi S4800 field-emission scanning electron microscopy (FESEM, 20 kV) and JEM-1011 transmission electron microscope (TEM, 100 kV). X-ray photoelectron spectroscopy (XPS) was obtained to examine the compositions and chemical states of the samples on a PHI5000 Versa Probe spectrometer with an Al K α as an X-ray source. The absorption spectrum was conducted with a UV-vis-NIR spectrometer (Shimadzu, UV-3600) in the range from 200 nm to 800 nm. The SERS spectra were recorded from the Reflex Confocal microRaman spectroscopy system (inVia, Renishaw, UK) with a 633 nm excitation wavelength and a 20 \times Nikon objective. The spectra of each sample were collected in the 600-1800 cm⁻¹ range with

an exposure time of 10 s and a laser power of 1.7 mW. All the Raman spectra have been averaged over the signals collected at five points chosen at random.

Synthesis of the Cu₂O templates.

A modified method was used to fabricate the octahedral-shaped Cu₂O templates.^{1, 2} In a general procedure, 170.5 mg of CuCl₂·2H₂O and 5.0 mg of the PVP-K30 were added into 100 mL of water together at 55 °C with vigorous stirring. And then, NaOH solution (10.0 mL, 2.0 M) was mixed into the above solution drop by drop and stirred for 30 min. At last, AA solution (10.0 mL, 0.6 M) was added to the mixture, and the mixture was stirred for 3 h. To further purify the product, the precipitated material was separated by centrifugation, washed with deionised water and ethanol repeatedly, and then dried under vacuum at 60°C overnight for subsequent characterization and analysis.

Fabrication of the hollow Ag superstructures.

The hollow Ag superstructures were synthesized by hard-templating method¹. First, 5.0 mg of the Cu₂O templates were mixed with 100 mL of ultrapure water under ultrasonic vibration. Then, the growth solution for Ag shells was started by adding TSC solution (1.0 mL 0.03 M) and ice-cold NaBH₄ aqueous solution (1.05 mL, 0.1 M) in the Cu₂O dispersion solution sequentially with stirring for 10 min. Next, AgNO₃ aqueous solution (1.05 mL, 0.01M) was injected into the vigorously stirred solution. A bright yellow appearance of the solution indicates the formation of Ag nanoparticles. During the reaction over 60 min, the color of the mixture slowly changed to dark yellow, suggesting the generation of Cu₂O@Ag. Subsequently, the Cu₂O templates were etched using an aqueous solution of CH₃COOH (1.7 mL, 1wt%) as a template remover. The reaction was continued for a further 120 minutes. The precipitated samples were recovered by centrifugation, washed repeatedly with distilled water and absolute ethanol, and finally redispersed in absolute ethanol for further analysis.

Preparation of close-packed hollow Ag superstructures.

A densely packed Ag superstructures were formed *via* self-assembly at the water/hexane surface driven by interfacial tension^{3, 4}. Typically, 6.0 mL of distilled

water and 2.0 mL of hexane were mixed in a 10.0 ml beaker to form the water/oil interface. Then, 2.0 mL of the Ag superstructures ethanol solution was added to the mixed solution drop by drop. The Ag superstructures then moved and stayed at the boundary region between the two phases, aggregating to produce a densely packed film. After removing most of this hexane with an aspirator, it was easy to transfer the film onto PDMS. A piece of PDMS was immersed into the solution with a small angle and pulled out slowly. After the natural evaporation of the hexane, the close-packed hollow Ag superstructures film was successfully transferred to the PDMS substrate. Thus, a flexible SERS chip modified with hollow Ag superstructures film was fabricated. For later use, the prepared SERS chip was stored in a desiccator and vacuum bags.

SERS measurement of the probes on substrates.

Molecules such as CV, MB, MG, and CuPc were used to evaluate the SERS behaviors of different substrates. Then 10 μ L of Raman molecule solution was added to the fabricated substrate and dried at 60 $^{\circ}$ C for 30 min before the Raman measurements.

Synthesis of the Ag nanoparticles.

The classic citric acid reduction method was adapted to synthesise the Ag nanoparticles with some modification. 1mL of TSC solution (2 wt%) was dropped into 49 mL of boiled AgNO₃ solution (1 mM) with stirring for 30 min. As the solution turned dark yellow, the Ag nanospheres were generated.

The calculations of enhancement factor (EF).

The enhancement factor (EF) was calculated to estimate the potentiation of the proposed substrate according to the following equations ^{5, 6}:

$$EF = \frac{I_{SERS}}{I_{bulk}} \times \frac{N_{bulk}}{N_{SERS}} \quad (1)$$

Where I_{SERS} and I_{bulk} represent the peak intensities of SERS and the normal Raman at 1622 cm^{-1} . Simultaneously, N_{SERS} and N_{bulk} are the valid molecule number on the self-assembled hollow Ag octahedron substrate and the practical number of probe molecules in the Raman detection view.

The number of probe molecules (N_{bulk}) in standard Raman detection can be calculated in the following equation:

$$N_{bulk} = \frac{\rho h S_{Raman} N_A}{M} \quad (2)$$

$$S_{Raman} = \pi \left(\frac{d_{laser}}{2} \right)^2 \quad (3)$$

$$d_{laser} = \frac{1.22\lambda}{N.A.} \quad (4)$$

$$h = \frac{3.28\eta d_{laser}}{N.A.} \quad (5)$$

Where S_{Raman} is the laser radiation area, M is the molecular weight (373.9 g mol⁻¹) and N_A is the Avogadro constant. In equation (4), d_{laser} is the diameter of the laser, and it could be inferred from equation (4). In equation (4), λ is the wavelength of the laser (633 nm) and $N.A.$ represents the numerical aperture of 20× objective ($N.A. = 0.4$). As for the laser radiation depth, η is the refractive index of water (1.33). ρ is the density of bulk MB (1.0 g cm⁻³) and h is the laser radiation depth, which could be calculated in equation (5) to be 21 μm. The peak intensities of the MB (1 × 10⁻² M, aqueous solution) directly dropped on bare glass were detected as Raman data. At last six points were randomly selected for continuous testing and averaged to reduce measurement error. Given that the molecules were distributed in a monolayer on the substrate, and the valid probe number on the self-assembled hollow Ag octahedron substrate in the SERS detection can be calculated using the following equation:

$$N_{SERS} = n N_A \frac{S_{SERS}}{S_{substrate}} = C V N_A \frac{S_{SERS}}{S_{substrate}} \quad (6)$$

Where, n is the the molar quantity of MB, C is the molar concentration of the analyte solution, V is the volume of the droplet, N_A is the Avogadro constant, S_{SERS} is the area of laser radiation in SERS detection, similar to S_{Raman} in the same conditions. $S_{substrate}$ is the area of the substrate (0.25 cm²).

The calculation of limit of detection (LOD) and relative standard deviation (RSD)

According to the formula $LOD = 3\sigma/S$, where σ and S represent the standard deviation of the blank samples and the slope of the line (at least 3 times), respectively.

For the calculation of relative standard deviation (RSD) spot-to-spot on the SERS chip, the SERS chip was tested for sensing 10^{-6} MB and 30 spectra were randomly collected from each sample and the average values were used for the RSD calculation.

Adsorption capacity.

To investigate the adsorption capacity (q) of the substrates, 1 mg of Ag nanoparticles and hollow Ag octahedrons were immersed in an MB solution (2 mL, 10^{-5} M) for 1 h in the dark. Then the liquid supernatant was isolated to evaluate the loading capacity. The amount of absorbed MB was confirmed by UV-vis spectrophotometer.

$$q = \frac{(C_0 - C_t)V}{m} \quad (7)$$

where C_0 is the initial concentration of MB, C_t is the absorbance concentration after 1 h, V is the volume of MB and m is the weight of Ag samples.

SERS detection of CIP, AMX and CZL in different water samples.

The wastewater from Xianlin water treatment plant (Nanjing) and tap water samples were first filtered through a 0.22 μ m filter before use and subsequently used as dispersing agents to obtain antibiotic solutions with a certain concentration.

SERS detection of ENR in milk.

To eliminate the interference of other substances with the signal, the obtained milk was pretreated according to previous reports. First, the milk was centrifuged at 11000 rpm for 15 min under 5°C . Then, 5.0 mL of supernatant was mixed with 4.5 mL of trichloroacetic acid (3%), and the liquid was shaken for 200 s. Next, the mixture was centrifuged under 9500 rpm for 10 min, and the supernatant was collected. The final pH of the supernatant was adjusted to ~ 7 using NaOH solution and the solution was subsequently filtered using a 0.22 μ m filter. The filtrate was diluted to 10 mL for subsequent ENR detection.

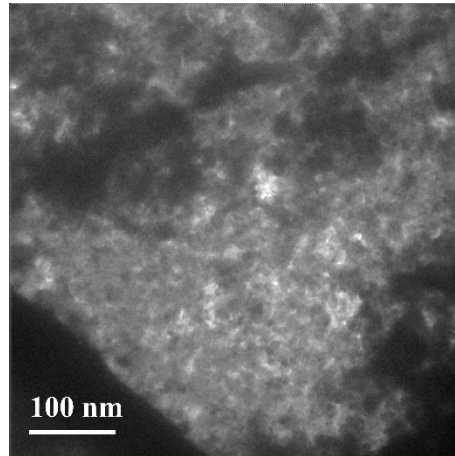


Fig. S1 The magnified TEM image of the hollow Ag octahedron.

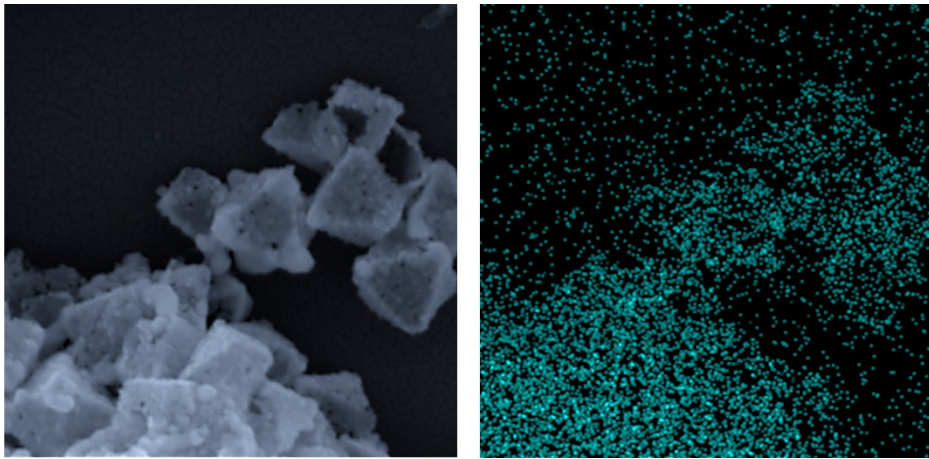


Fig. S2 The EDX mapping of hollow Ag octahedron.

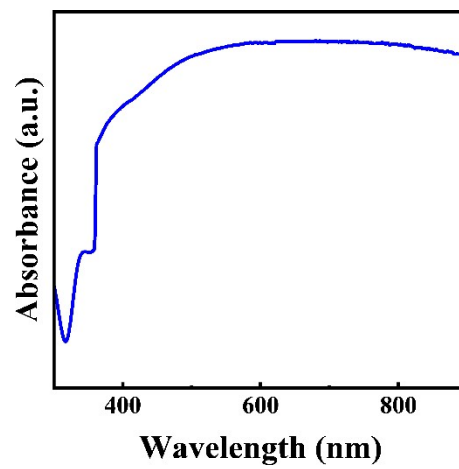


Fig. S3 The UV-vis spectrum of hollow Ag octahedron.

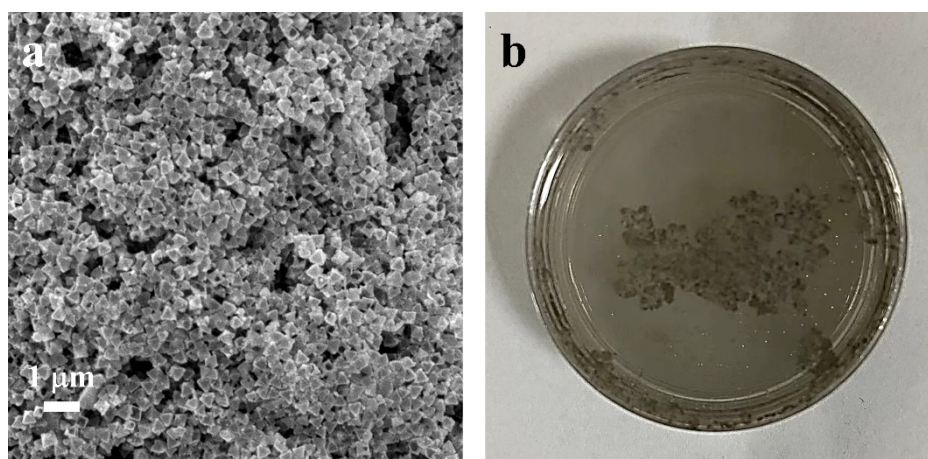


Fig. S4 The (a) SEM image and (b) photo of a self-assembled hollow Ag octahedron.

The SEM image and picture in Fig. S4 demonstrated the self-assembled hollow Ag octahedron. this mode allows the formation of additional hot spots, further enhancing the Raman signal.

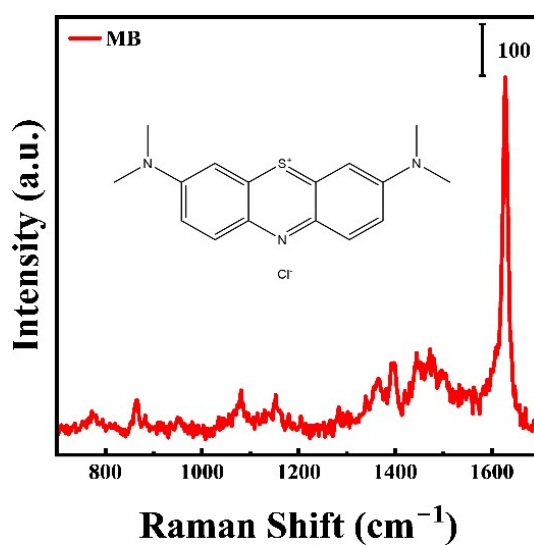


Fig. S5 The Raman spectrum and chemical formula of MB.

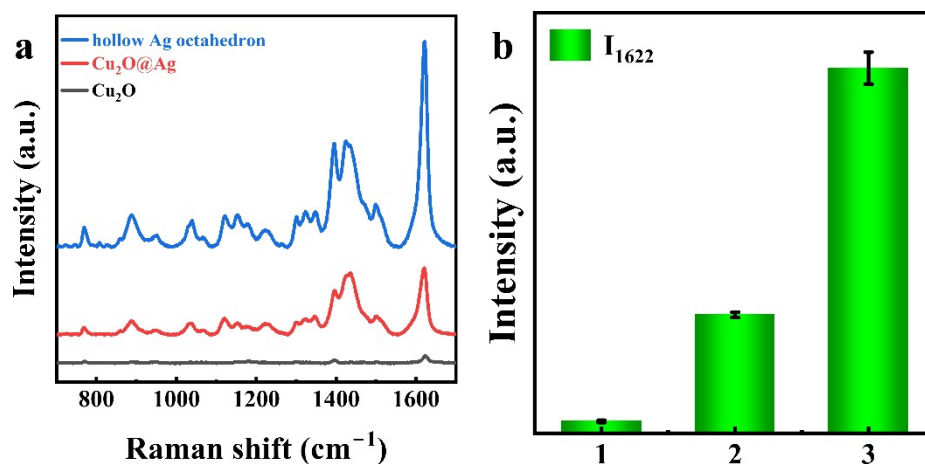


Fig. S6 The Raman spectra of MB (10^{-5} M) absorbed on the Cu₂O, Cu₂O@Ag and hollow Ag octahedron. (b) The intensity of characteristic peak at 1622 cm⁻¹ in (a). The numbers 1, 2 and 3 represent Cu₂O, Cu₂O@Ag and hollow Ag octahedron, respectively.

As depicted in Fig. S6, noticeable differences in the SERS performance were observed among these samples. the hollow Ag octahedron exhibited the most significant Raman enhancement performance compared to pure Cu₂O and Cu₂O @Ag. such a considerable enhancement derives from loading more Raman molecules and the multiple scattering of light due to the unique structure.

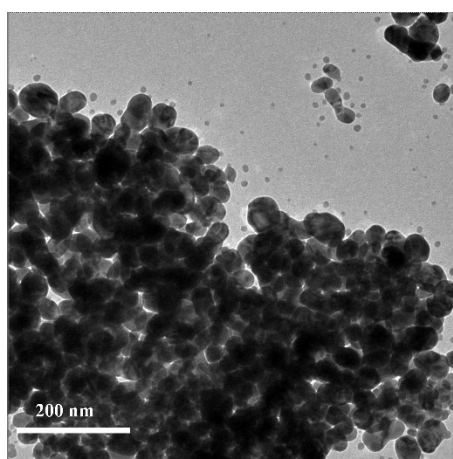


Fig. S7 The TEM image of Ag nanoparticles.

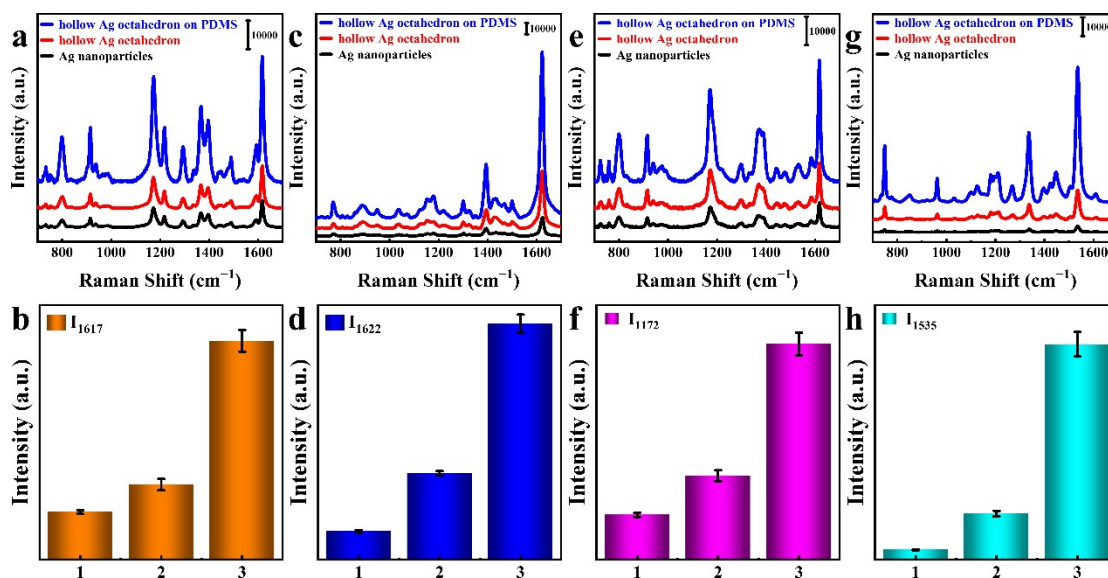


Fig. S8 The Raman spectra and the corresponding intensity of fingerprint peak of (a, b) MG (10^{-5} M), (c, d) MB (10^{-5} M), (e, f) CV (10^{-5} M) and (g, h) CuPc (10^{-5} M) on the Ag nanoparticles (black line), hollow Ag octahedron (red line) and the self-assembled hollow Ag octahedron (blue line).

When compared to Ag nanoparticles and hollow Ag octahedrons, the signal strength of the characteristic peak of MB was 4.6 and 2.9 times higher, that of MG 8.4 and 2.7 times higher, that of CV 4.8 and 2.6 times higher, and that of CuPc 22.3 and 4.6 times higher on the proposed SERS chips, respectively.

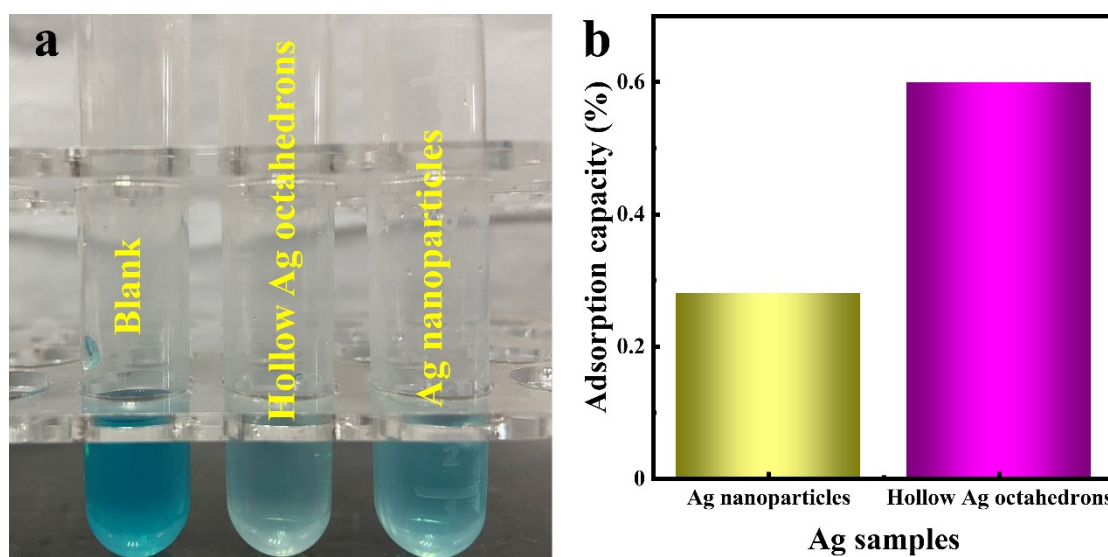


Fig. S9 (a) The photograph of MB solution (1×10^{-5} M) after absorbed by different Ag samples for 1 h in dark and (b) the adsorption capacity (q) of the Ag samples.

The photograph in Fig. S9 demonstrate that hollow Ag octahedrons have higher adsorption capacity than Ag nanoparticles, indicating its strong enrichment ability for molecules.

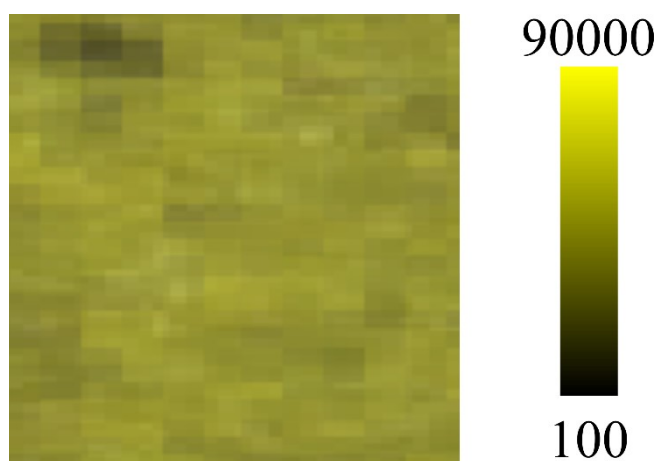


Fig. S10 SERS mapping of MB (1×10^{-6} M) at the characteristic peak 1622 cm^{-1} absorbed on self-assembled hollow Ag octahedron substrates.

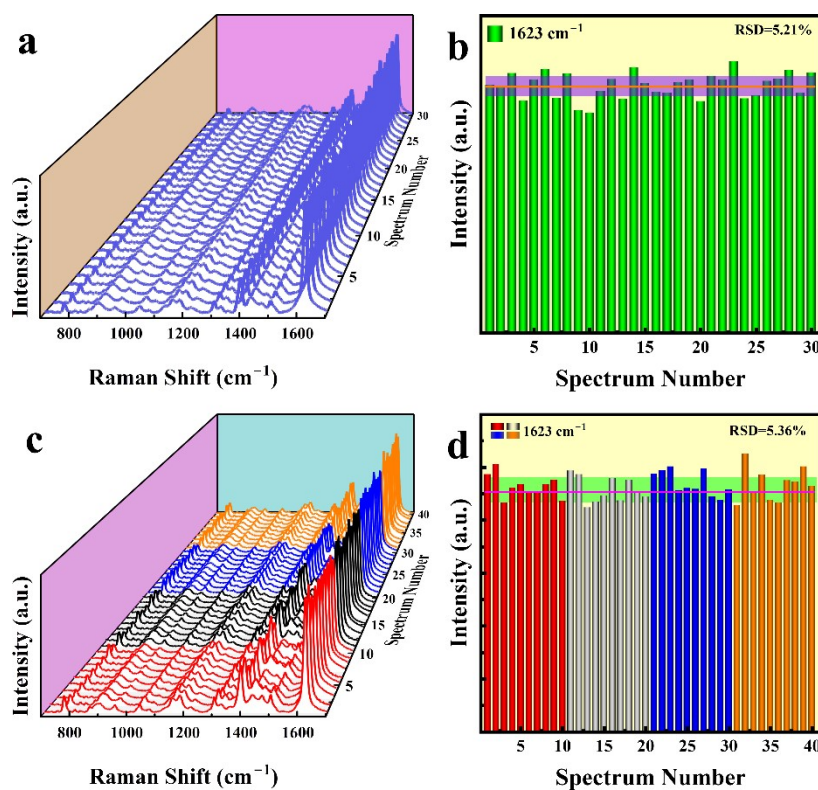


Fig. S11 (a) SERS spectra of MB (10^{-6} M) on the self-assembled hollow Ag octahedron from 30 randomly selected spots and (b) the corresponding histogram of peak intensity at 1622 cm^{-1} . (c) SERS spectra of MB (10^{-6} M) on four batches (No. 1-10: 1st batch, No. 11-20: 2nd batch, No. 21-30: 3rd batch, No. 31-40: 4th batch) of the self-assembled hollow Ag octahedron from randomly selected spots and (d) the corresponding histogram of peak intensity at 1622 cm^{-1} .

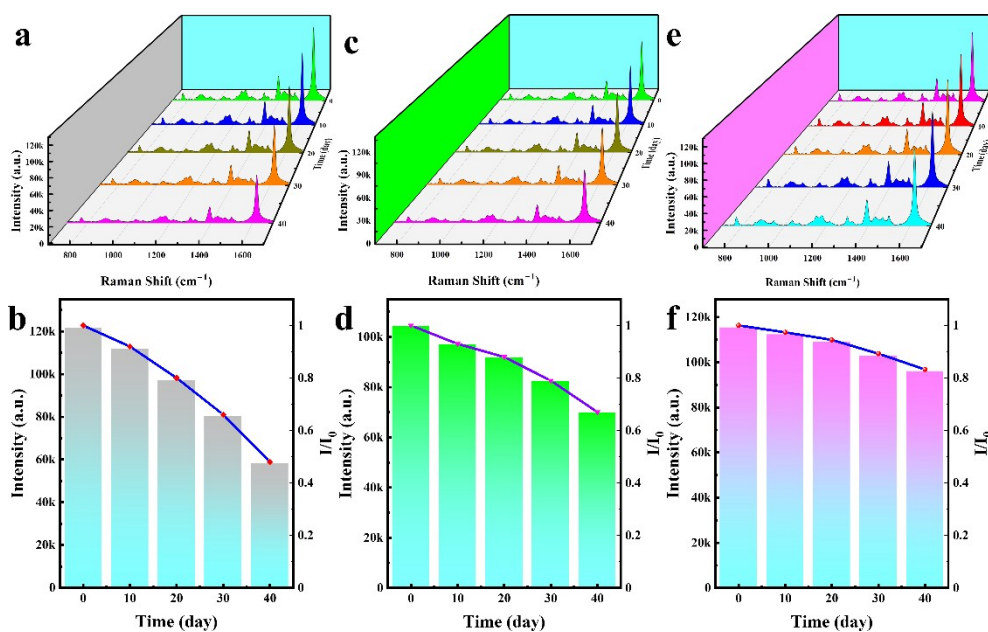


Fig. S12 (a) SERS signals of MB on the SERS chip exposure to air condition during 40 days and (b) the corresponding histogram of peak intensity at 1622 cm^{-1} . (c) SERS signals of MB on the SERS chip placed in a desiccator condition for 40 days and (d) the corresponding histogram of peak intensity at 1622 cm^{-1} . (e) SERS signals of MB on the SERS chip preserved in vacuum bags for 40 days and (f) the corresponding histogram of peak intensity at 1622 cm^{-1} .



Fig. S13 The photograph of substrates preserved in vacuum packaging.

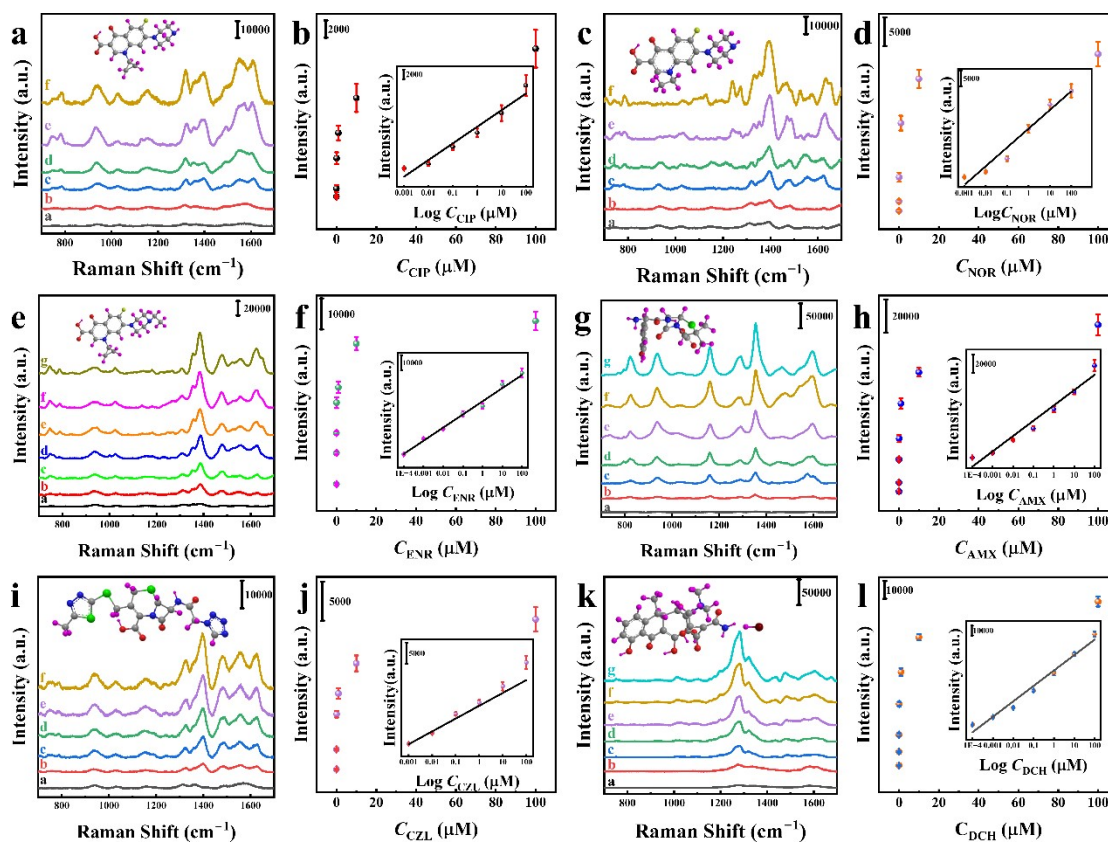


Fig. S14 SERS spectra of antibiotics and the corresponding scatter plot with calibration curve (inset) at different concentrations based on closely packed hollow silver octahedron and. (a and b) CIP solution (μM) with various concentrations from 10^{-4} to 10^{-10} M, (c and d) NOR solution with various concentrations from 10^{-4} to 10^{-9} M, (e and f) ENR solution with multiple concentrations from 10^{-4} to 10^{-10} M, (g and h) AMX solution with various concentrations from 10^{-4} to 10^{-10} M, (i and j) CZL solution with various concentrations from 10^{-4} to 10^{-9} M, (k and l) DCH solution with various concentrations from 10^{-4} to 10^{-10} M.

As shown in Fig. S14, the Raman signal intensity of the applied amplified gradually with the increase in concentration (from line a to f/g). Whatever the type of antibiotic molecule, sensitive detection was obtained over wide ranges.

Table S1 Comparisons of the limit of detection (LOD) for MB and EF among different SERS substrates

No.	SERS substrate	Raman probe	EF	LOD (M)	Ref.
1	Ag/TiO ₂	MB	1.4×10 ⁸	1.0×10 ⁻⁸	7
2	MoS ₂ @ZnO _{1:4}	MB	1.1×10 ⁶	1.0×10 ⁻¹²	8
3	Ag NCs/ chitosan	MB	1.4×10 ⁶	1.0×10 ⁻⁹	9
4	MoS ₂	MB	3.56×10 ⁵	1.0×10 ⁻⁷	10
5	Closed –packed hollow Ag octrahedron	MB	3.6×10 ⁷	3.4 ×10 ⁻¹³	This work

Table S2 Comparisons of the LOD for MB with different methods

Method	Linear range (M)	LOD (M)	Ref.
Electrochemistry	1.0×10^{-8} - 5.0×10^{-5}	2.1×10^{-10}	11
Electrochemistry	1.0×10^{-7} - 1.0×10^{-3}	4.7×10^{-9}	12
SERS	1.0×10^{-7} - 1.0×10^{-3}	1.0×10^{-7}	13
SERS	1.0×10^{-12} - 1.0×10^{-6}	3.4×10^{-13}	This work

Table S3 Comparisons of the storage time with Ag-related SERS substrates.

Substrate name	Storage time (day)	Ref.
Ag nanoparticles/ Bacterial Nanocellulose	20	14
Ag nanoparticles/carbon aerogels	28	15
TiO ₂ -Ag-GO	20	16
Closed -packed hollow Ag octrahedron	40	This work

The SERS chip that we have designed has an improved time stability in comparison to other SERS substrates that are Ag-related.

Table S4 The linear equations, R² and LOD of different antibiotics

Analyte	Linear equation	R ²	LOD (nM)
CIP	$y=(9908\pm 630)+(3439\pm 354) \log C_{\text{CIP}}$	0.960	0.60
NOR	$y=(18382\pm 1051)+(6001\pm 590) \log C_{\text{NOR}}$	0.962	0.21
ENR	$y=(38675\pm 1798)+(8648\pm 549) \log C_{\text{ENR}}$	0.981	0.058
AMX	$y=(58760\pm 3328)+(16740\pm 1488) \log C_{\text{AMX}}$	0.961	0.063
CZL	$y=(10922\pm 391)+(3747\pm 219) \log C_{\text{CZL}}$	0.986	0.72
DCH	$y=(59691\pm 2397)+(15579\pm 1072) \log C_{\text{DCH}}$	0.977	0.057

We then plotted the intensities at the characteristic peaks against the logarithm of the concentration to get the fitted line profile. The linearity between Raman intensity and log concentration was excellent for CIP from 10⁻⁴ to 10⁻⁹ M, for NOR from 10⁻⁴ to 10⁻⁹ M, for ENR from 10⁻⁴ to 10⁻¹⁰ M, for AMX from 10⁻⁴ to 10⁻¹⁰ M, for CZL from 10⁻⁴ to 10⁻⁹ M, for DCH 10⁻⁴ to 10⁻¹⁰ M, respectively. The detailed correlation equations, as well as R² and LOD, are listed in Table S3. The LODs are calculated to be 0.6 nM for CIP, 0.21 nM for NOR, 0.058 nM for ENR, 0.063 nM for AMX, 0.72 nM for CZL, and 0.057 nM for DCH.

Table S5 Comparisons with previous methods for different antibiotics

Target	Method	Linear range (M)	LOD (M)	Ref.
CIP	Fluorescence	1.0×10^{-6} - 1.0×10^{-4}	6.0×10^{-6}	17
	Fluorescence	0- 1.2×10^{-4}	6.0×10^{-7}	18
	Electrochemistry	7.5×10^{-8} - 1.0×10^{-5}	4.0×10^{-8}	19
	Electrochemistry	2.0×10^{-8} - 1.2×10^{-4}	2.0×10^{-8}	20
	SERS	1.0×10^{-9} - 1.0×10^{-4}	6.0×10^{-10}	This work
NOR	Electrochemistry	4.6×10^{-10} - 9.7×10^{-4}	4.6×10^{-10}	21
	Fluorescence	3.1×10^{-9} - 3.1×10^{-7}	1.1×10^{-9}	22
	Colorimetry	1.2×10^{-6} - 8.0×10^{-6}	2.0×10^{-7}	23
	SERS	9.4×10^{-9} - 1.6×10^{-6}	2.5×10^{-9}	24
	SERS	1.0×10^{-9} - 1.0×10^{-4}	2.1×10^{-10}	This work
ENR	Chemiluminescence	9.7×10^{-10} - 2.7×10^{-6}	8.4×10^{-11}	25
	Fluorescence	5.0×10^{-9} - 2.5×10^{-7}	3.7×10^{-8}	26
	Electrochemistry	2.7×10^{-9} - 2.7×10^{-6}	5.6×10^{-10}	27
	SERS	1.0×10^{-10} - 1.0×10^{-4}	5.8×10^{-11}	This work
AMX	SERS	1.0×10^{-9} - 1.0×10^{-4}	1.0×10^{-9}	28
	Fluorescence	5.0×10^{-6} - 1.0×10^{-4}	3.4×10^{-11}	29
	Electrochemistry	3.0×10^{-7} - 5.0×10^{-4}	3.0×10^{-7}	30
	SERS	1.0×10^{-10} - 1.0×10^{-4}	6.3×10^{-11}	This work
CZL	Chemiluminescence	4.4×10^{-8} - 4.4×10^{-6}	1.0×10^{-8}	31
	Chemiluminescence	2.5×10^{-8} - 3.0×10^{-7}	9.6×10^{-9}	32
	Fluorescence	1.7×10^{-9} - 2.6×10^{-8}	1.2×10^{-9}	33
	SERS	1.0×10^{-9} - 1.0×10^{-4}	7.2×10^{-10}	This work
DCH	Fluorescence	1.0×10^{-8} - 5.0×10^{-6}	6.5×10^{-10}	34
	Fluorescence	5.0×10^{-8} - 1.4×10^{-5}	6.4×10^{-9}	35
	Colorimetry	1.0×10^{-6} - 7.3×10^{-5}	5.0×10^{-9}	36
	SERS	1.0×10^{-10} - 1.0×10^{-4}	5.7×10^{-11}	This work

Table S6 Determination of ENR in milk by standard addition method

Sample	Spiked (μM)	Detected (μM)	Recovery (n=3, %)	RSD (n=3, %)
1	0.01	0.0106	106	3.7727
2	0.1	0.0982	98.2	3.3488
3	1	1.0474	104.74	4.2016

As one of the most nutritious foods available, ensuring the quality and safety of milk is of utmost importance. Antibiotics are crucial in preventing and treating diseases when used as feed additives. However, human health and the environment are threatened by the overuse of antibiotics, as the drugs accumulate in animals and subsequently enter the human body and the ecosystem. Accordingly, residues of antibiotics in milk represent a pressing concern that warrants thorough discussion.

References

1. F. Huang, G. Ma, J. Liu, J. Lin, X. Wang and L. Guo, *Small*, 2016, **12**, 5442-5448.
2. J. Lin, W. Hao, Y. Shang, X. Wang, D. Qiu, G. Ma, C. Chen, S. Li and L. Guo, *Small*, 2018, **14**, 1703274.
3. H. Wang, W. Chen, B. Chen, Y. Jiao, Y. Wang, X. Wang, X. Du, Y. Hu, X. Lv, Y. Zeng, X. Wang, L. Qian and J. Xiong, *Small*, 2020, **16**, e1905480.
4. L. Xing, Y. Xiahou, X. Zhang, W. Du, P. Zhang and H. Xia, *ACS Appl. Mater. Interfaces*, 2022, **14**, 13480-13489.
5. T. Zheng, E. Feng, Z. Wang, X. Gong and Y. Tian, *ACS Appl. Mater. Interfaces*, 2017, **9**, 36596-36605.
6. Y. Zhou, Q. Gu, T. Qiu, X. He, J. Chen, R. Qi, R. Huang, T. Zheng and Y. Tian, *Angew. Chem. Int. Ed.*, 2021, **60**, 26260-26267.
7. H. Zhai, C. Zhu, X. Wang, Y. Yuan and H. Tang, *Front Chem*, 2022, **10**, 992236.
8. Y. Quan, J. Yao, Y. Sun, X. Qu, R. Su, M. Hu, L. Chen, Y. Liu, M. Gao and J. Yang, *Sensors and Actuators B: Chemical*, 2021, **327**, 128903.
9. B. M. Basavaraja, R. P. Bantwal, A. Tripathi, G. Hegde, N. S. John, R. Thapa, G. Hegde, R. G. Balakrishna, M. Saxena, A. Altaee and A. K. Samal, *ACS Sustain. Chem. Eng.*, 2023, **11**, 10605-10619.
10. R. Su, Y. Quan, S. Yang, M. Hu, J. Yang and M. Gao, *J. Alloys Compd.*, 2021, **886**, 161268.
11. M. Hayat, A. Shah, J. Nisar, I. Shah, A. Haleem and M. N. Ashiq, *Catalysts*, 2022, **12**, 306.
12. T.-C. Lin, Y.-S. Li, W.-H. Chiang and Z. Pei, *Biosens. Bioelectron.*, 2017, **89**, 511-517.
13. L. Que, J. Ai, T. Shao, R. Han, J. Su, Y. Guo, Y. Liu, J. Li, X. Jian and Z. Zhou, *Appl. Surf. Sci.*, 2023, **616**, 156496.
14. N. Chaudhary, D. Verma, J. Gopal Sharma and P. R. Solanki, *Mater. Lett.*, 2022,

- 308**, 131090.
15. H. Xia, M. Peng, N. Li and L. Liu, *Chem. Phys. Lett.*, 2020, **740**, 137085.
 16. M. Sabeti, A. A. Ensafi, K. Z. Mousaabadi and B. Rezaei, *IEEE Sens. J.*, 2021, **21**, 19714-19721.
 17. K. Mariappan, S. Alagarsamy, S.-M. Chen and S. Sakthinathan, *Materials*, 2023, **16**, 741.
 18. O. T. Vu, Q. H. Nguyen, T. Nguy Phan, T. T. Luong, K. Eersels, P. Wagner and L. T. N. Truong, *ACS Omega*, 2023, **8**, 2887-2896.
 19. O. Bunkoed, P. Donkhampa and P. Nurerk, *Microchem. J.*, 2020, **158**, 105127.
 20. Y. Song, J. Qiao, W. Liu and L. Qi, *Anal. Bioanal. Chem.*, 2021, **413**, 979-985.
 21. H. Zhang, X. Fan, Y. Ding, L. Yi, K. Ge and Y. Gu, *Food Chem.*, 2023, **429**, 136928.
 22. F. Yu, S. Yu, L. Yu, Y. Li, Y. Wu, H. Zhang, L. Qu and P. d. B. Harrington, *Food Chem.*, 2014, **149**, 71-75.
 23. S. Dolati, M. Ramezani, M. S. Nabavinia, V. Soheili, K. Abnous and S. M. Taghdisi, *Anal. Biochem.*, 2018, **549**, 124-129.
 24. Y. Song, M. Xu, X. Liu, Z. Li, C. Wang, Q. Jia, Z. Zhang and M. Du, *Electrochim. Acta*, 2021, **368**, 137609.
 25. G. Dikmen, *Spectrochimica Acta Part A: Molecular and Biomolecular Spectroscopy*, 2022, **278**, 121308.
 26. X.-R. Guo, Y.-M. Dong, X.-Y. Chen and J. Chen, *Spectrochimica Acta Part A: Molecular and Biomolecular Spectroscopy*, 2022, **282**, 121703.
 27. S. R. Sari, E. Shinchu, K. Shida, Y. Kusumawati, K. A. Madurani, F. Kurniawan and M. Tominaga, *Analyst*, 2023, **148**, 2932-2940.
 28. H. Sun, J. Wang and T. Wang, *Luminescence*, 2013, **28**, 592-596.
 29. R. Salari, M. Amjadi and T. Hallaj, *Spectrochimica Acta Part A: Molecular and Biomolecular Spectroscopy*, 2023, **285**, 121845.
 30. S. Rastegarzadeh, M. Kalantaripour and N. Pourreza, *Anal. Sci.*, 2023, **39**, 257-266.

31. M. S. Attia, W. H. Mahmoud, M. N. Ramsis, L. H. Khalil, A. M. Othman, S. G. Hashem and M. S. Mostafa, *Journal of Fluorescence*, 2011, **21**, 1739-1748.
32. Y. Fan, W. Yu, Y. Liao, X. Jiang, Z. Wang and Z. Cheng, *Spectrochimica Acta Part A: Molecular and Biomolecular Spectroscopy*, 2022, **267**, 120509.
33. J. O. Abdulsattar, H. Hadi, S. Richardson, A. Iles and N. Pamme, *Anal. Chim. Acta*, 2020, **1136**, 196-204.
34. S. Zhang, J. Xu, Y. Huang, Z. Liu and S. Jiang, *ACS Appl. Nano Mater.*, 2022, **5**, 18519-18530.
35. C. Zheng, J. Yu, L. Dou, Z. Wang, Z. Huang, X. Li, X. Hu and Y. Li, *ACS Appl. Mater. Interfaces*, 2023, **15**, 29609-29617.
36. M. Zhang, H. Sun, X. Chen, H. Zhou, L. Xiong, W. Chen, Z. Chen, Z. Bao and Y. Wu, *J. Alloys Compd.*, 2021, **864**, 158189.